may reflect adaptations promoting gas exchange in low-oxygen environments within the sediment as well, as the shapes of species with subsurface maxima have higher surface area/volume ratios than the epifaunal species.

The distribution of live benthic foraminifera within these deep-sea sediments suggests that certain foraminifera with infaunal microhabitats are not directly controlled by overlying bottom-water conditions, but by physicochemical conditions within the sediment, as this environment is geochemically different from the sediment/water interface[26-28]. Some species do not appear to be confined to infaunal habitats, but instead are responding to a set of physicochemical variables independent of sediment depth. For example, *Chilostomella* and *Globobulimina* are found at depth in OC-86/2-7-4, but related species are common in California Borderland surface sediments (based on Rose Bengal stained data) associated with bottom water dissolved-oxygen values of <3 ml l^{-1} and generally <1 ml l^{-1} (ref. 29). The depth distribution of a particular species probably varies regionally in response to different physicochemical conditions within the sediments, ontogenetic differences in microhabitat requirements, or as a result of seasonal cycles in the deep sea.

Recent carbon-isotope data from pore waters in the upper few centimetres of Pacific Ocean and Atlantic Ocean sediments (ref. 30 and F. L. Sayles and W. B. Curry, in preparation) indicate that a $\delta^{13}C$ gradient of $\sim 1‰$ exists in the upper one to a few centimetres. The $\delta^{13}C$ values decrease with depth in the sediment because of the oxidation of ^{12}C-enriched organic matter, which results in a decrease in the $\delta^{13}C$ of the pore waters. The demonstration from the OC-86/2 data that a number of deep-sea benthic foraminifera do have infaunal microhabitats, together with the existence of $\delta^{13}C$ gradients within deep-sea sediments, indicate that the $\delta^{13}C$ disequilibrium of some benthic foraminifera can probably be explained in part by the $\delta^{13}C$ composition of the pore waters. Benthic foraminiferal carbon-isotope data[10,11,13,31] show that plano-convex or biconvex forms, inferred to be epifaunal species, are generally nearest to isotope equilibrium, whereas species with shapes suggesting infaunal habitats are depleted in ^{13}C. For example, a species of *Globobulimina* was highly variable with $\delta^{13}C$ up to 2-3‰ below equilibrium of the overlying bottom water in the California Borderlands[12]. One notable exception to this pattern, however, is *O. tener*, which has consistently lighter values than other biconvex forms. The existing data suggest that a relationship exists between carbon isotope composition and test morphology, which would be expected if the pore-water geochemistry of the microenvironment influences the benthic foraminiferal carbon-isotope data.

I thank L. D. Keigwin Jr, W. B. Curry, S. Honjo and F. L. Sayles for discussions on the research; W. A. Berggren, W. B. Curry, S. R. Emerson, L. D. Keigwin Jr and G. Vilks for reviewing the manuscript; E. L. Grossman for a preprint of his isotope work; J. W. Farrington, B. W. Tripp and C. H. Clifford for obtaining box-core subsamples; M. H. Jeglinski for picking the foraminifera; E. Evans and Joyce Graves for typing the manuscript; T. A. L. Corliss for assistance in verifying the living specimens. This research was supported by grants from the Center for Analysis of Marine Systems, Woods Hole Oceanographic Institution and from a consortium of oil companies (Atlantic-Richfield Co., British Petroleum Corp., Chevron U.S.A. Inc., Cities Service, Elf-Aquitaine, Exxon Production Research Co., Gulf Oil Co., Mobil Oil Corp., Phillips Petroleum, Shell Oil Co. (International), Shell Oil Co. (USA), Texaco Inc., Union Oil Company of California). This is Woods Hole Oceanographic Institution Contribution no. 5729.

Received 24 October; accepted 18 December 1984.

1. Bandy, O. L. *21st Int. geol. Congr.*, Copenhagen, Pt 22, 7-25 (1960).
2. Barr, F. T. & Berggren, W. A. in *The Geology of Libya* (eds Salem, M. J. & Busrewil, M. T.) 163-192 (Academic, New York, 1981).
3. Berggren, W. A. & Aubert, J. *Geol. Surv. prof. Pap.* **1213**, 4-21 (1983).
4. Douglas, R. G. & Woodruff, F. in *The Sea* Vol. 7 (ed. Emiliani, C.) 1233-1327 (Wiley-Interscience, New York, 1981).
5. Shackleton, N. J. & Opdyke, N. D. *Quat. Res.* **3**, 39-55 (1973).
6. Shackleton, N. J. & Opdyke, N. D. *Geol. Soc. Am. Mem.* **145** (eds Cline, R. M. & Hays, J. D.) 449-464 (1976).
7. Boyle, E. A. & Keigwin, L. D. Jr *Science* **218**, 784-787 (1982).
8. Curry, W. B. & Lohmann, G. P. *Nature* **306**, 577-580 (1983).
9. Shackleton, N. J., Imbrie, J. & Hall, M. A. *Earth planet. Sci. Lett.* **65**, 233-244 (1983).
10. Woodruff, F., Savin, S. M. & Douglas, R. G. *Mar. Micropaleont.* **5**, 3-11 (1980).
11. Belanger, P. E., Curry, W. B. & Matthews, R. K. *Palaeogeogr., Palaeoclimatol., Palaeoecol.* **33**, 205-220 (1981).
12. Grossman, E. L., *Palaeogeogr., Palaeoclimatol., Palaeoecol.* **47**, 301-327 (1984).
13. Graham, D. W., Corliss, B. H., Bender, M. L. & Keigwin, L. D. Jr *Mar. Micropaleont.* **6**, 483-497 (1981).
14. Savin, S. M. *et al. Mar. Micropaleont.* **6**, 423-450 (1981).
15. Keigwin, L. D. Jr *Init. Rep. DSDP* **68**, 445-453 (1982).
16. Boltovskoy, E. & Wright, R. *Recent Foraminifera*, 1-515 (Junk, The Hague, 1976).
17. Boltovskoy, E. *Contr. Cushman Fdn Foraminifera Res.* **17**, 43-45 (1966).
18. Brooks, A. L. *Limnol. Oceanogr.* **12**, 667-684 (1967).
19. Schafer, C. T. *Limnol. Oceanogr.* **16**, 944-951 (1971).
20. Ellison, R. L. *Geol. Soc. Am. Mem.* **133**, 247-262 (1972).
21. Matera, N. J. & Lee, J. J. *Mar. Biol.* **14**, 89-103 (1972).
22. Frankel, L. *J. Paleont.* **46**, 62-65 (1972).
23. Frankel, L. *J. Paleont.* **49**, 563-565 (1975).
24. Ellison, R. L. & Peck, G. E., *J. Foram. Res.* **13** (4), 231-241 (1983).
25. Leutenegger, S. & Hansen, H. J. *Mar. Biol.* **54**, 11-16 (1979).
26. Froelich, P. N. *et al. Geochim. cosmochim. Acta* **43**, 1075-1090 (1979).
27. Berner, R. R. in *The Environment of the Deep Sea* (eds Ernst, W. G. & Morin, J. G.) 154-176 (Prentice-Hall, Hemel Hempstead, 1982).
28. Sayles, F. L. *Geochim. cosmochim. Acta* **45**, 1061-1086 (1981).
29. Douglas, R. G. & Heitman, H. L. *SEPM spec. Publ.* **27**, 231-246 (1979).
30. McCorckle, D. C. & Emerson, S. R. *EOS* **64**, 721 (1983).
31. Shackleton, N. J., Hall, M. A. & Boersma, A. *Init. Rep. DSDP.* **74**, 599-612 (1984).

Weak neutral currents and the origin of biomolecular chirality

D. K. Kondepudi & G. W. Nelson

Center for Statistical Mechanics and Thermodynamics, The University of Texas, Austin, Texas 78712, USA

It has long been known that Earth's biochemistry is overwhelmingly dissymmetric or chiral[1-4]. In model chemical systems[5-7] that spontaneously evolve to a state dominated by either the L or the D enantiomer, parity violation in β-decay and that attributable to weak neutral currents (WNC) in molecules[8,9] is thought to be too small to have any significant influence on the emergent chirality[10,11]. Other conceivable systematic chiral influences are generally even weaker[12-14]. We show here that there is a simple and extremely sensitive mechanism by which a minute but systematic chiral interaction, no stronger than the WNC interaction in amino acids, can, over a period of $\sim 15{,}000$ yr, determine which enantiomer will dominate. Such a mechanism is especially interesting when considering the origins of terrestrial biochemistry, particularly in view of the work by Mason and Tranter[15], who found that it is the terrestrially dominant L amino acids that are favoured by the WNC interaction.

The process occurs in a randomly fluctuating environment. Chemical systems that, in conditions that are thermodynamically far from equilibrium, can evolve spontaneously to a chirally asymmetric state—that is 'break chiral symmetry'—exhibit a universal behaviour that is a consequence of the symmetry properties of the system[14,16-18]. The amplitude α of the chiral dissymmetry, with the inclusion of fluctuations, obeys the stochastic (Langevin) equation

$$\frac{d\alpha}{dt} = -A\alpha^3 + B(\lambda - \lambda_c)\alpha + Cg + C'\eta f_2(t) + \varepsilon_1^{1/2} f_1(t) \quad (1)$$

in which A, B and C are constants that depend on the kinetics[14,16]; $g \equiv (\Delta E/kT)$, where k is the Boltzmann constant and T the temperature, is the factor by which the Arrhenius reaction rate constants for the L and the D enantiomers differ because of a small difference, ΔE, in their reaction barrier energies caused by an extremely weak chiral interaction[14]—such as WNC. In addition to such systematic effects, there is the fluctuating chiral influence from the environment, such as that attributable to circularly polarized ultraviolet light, represented by $C'\eta f_2(t)$, where $f_2(t)$ is assumed to be a normalized gaussian white noise. We estimate the numerical value of $C'\eta$ from the best known data on circularly polarized light. The intrinsic

thermodynamic fluctuations[19,20] are represented by $\varepsilon_1^{1/2} f_1(t)$; again $f_1(t)$ is assumed to be a normalized gaussian white noise; $\varepsilon_1 = (Q/VN_A)$, where Q can be calculated from the chemical kinetics; V is the volume over which the concentration of the reactants may be assumed homogeneous and N_A is the Avogadro number. The most general stochastic equation must include fluctuations in A and B but, as they have no significant effect on the mechanism[21,22], we ignore them.

As an example and for later numerical considerations, we shall consider the following model scheme of reactions studied in detail in ref. 14

$$S + T \underset{k_{-1}}{\overset{k_1}{\rightleftharpoons}} X_{L(D)} \qquad \text{(i)}$$

$$S + T + X_{L(D)} \underset{k_{-2}}{\overset{k_2}{\rightleftharpoons}} 2X_{L(D)} \qquad \text{(ii)}$$

$$X_L + X_D \xrightarrow{k_3} P. \qquad \text{(iii)}$$

In this scheme, the chiral species X in the two enantiomeric forms X_L and X_D is produced from the achiral substrate S and T directly through reaction (i) and autocatalytically through reactions (ii). With a suitable supply of S and T (to maintain their concentrations at a fixed level), and the irreversible removal of X through reaction (iii), the system can be driven far from thermodynamic equilibrium. The variables of equation (1) for this system are: $\lambda \equiv [S][T]$ and $\alpha \equiv ([X_L]-[X_D])/2$ (where [] denote concentrations). When λ exceeds a certain critical value λ_c, the steady-state value of α switches from zero to either $\alpha > 0$ or $\alpha < 0$ (ref. 14). If the small chiral interaction influences reactions (i) and (ii) so that the rate constants of the L and D enantiomers are unequal, $k_{1L} = k_{1D}(1+g)$ and $k_{2L} = k_{2D}(1+g)$, then $C = [k_1 + k_2\beta_c]\lambda_c$, where $\beta \equiv ([X_L]+[X_D])/2$, k_1 and k_2 are rate constants when $g = 0$, and the subscript 'c' denotes values at the critical point. Similar, but more involved, expressions may be obtained for A and B (ref.14).

In contrast to the earlier studies[23-25] that mainly examined such systems for $\lambda > \lambda_c$, we study the system as it slowly evolves through the critical point. The macroscopic steady states (when the fluctuations are ignored) and a sample fluctuating trajectory for the time evolution of α of equation (1) are shown in Fig. 1. When λ is well below λ_c, there is only one steady state, $\alpha \simeq Cg/B(\lambda - \lambda_c) \ll 1$, which becomes unstable when λ goes beyond λ_c; for $\lambda > \lambda_c$, the system has two new supercritical branches, $\alpha \simeq \pm\sqrt{B(\lambda - \lambda_c)/A}$, to which it can evolve. In the absence of g, the two supercritical branches emerge symmetrically (as a parabola) from the point λ_c and, as the system evolves through the critical point, the fluctuations make both states equally probable. When $g \neq 0$ this is no longer true; one branch is favoured. The effect of g is most marked in the vicinity of the critical point where it separates the two stable supercritical branches by a minimum of $S = (3/2)(4/A)^{1/3}(Cg)^{1/3}$; in contrast, well above and below the critical point the shift is proportional to Cg. As $Cg \ll 1$, the fractional exponent indicates the enhanced sensitivity of the system near the critical point. However, in this region the α fluctuations are also large. Our aim is to obtain the probability of the system evolving to the favoured branch as λ goes through the critical point at a given rate.

An important factor in calculating this probability is $\varepsilon_1 = Q/VN_A$, which is derived assuming the system is homogeneous over the volume V. We estimate V by considering the homogenization that occurs through diffusion and, for prebiotic considerations, large-scale mixing as might occur in an ocean or a lagoon.

The evolution of the system may be considered in four stages (see Fig. 1). In stages I and IV, the system is well below and well above the critical point respectively; during stages II and III, it is in the vicinity of the critical point where the selection of branches takes place. In stages I and II, there is only one stable steady state and hence the system can be homogeneous over limitlessly large volume. In stage II, if $\alpha \ll 1$ and $\lambda \simeq \lambda_c$, α begins to grow slowly, essentially at an average rate Cg. In stage III, however, the system has two possible steady states and hence the volume over which it may be assumed homogeneous has an upper limit. In this stage, in a small volume δV, the autocatalysis of the chemistry (reflected in the term $B(\lambda - \lambda_c)$, $\lambda > \lambda_c$) will cause a fluctuation in α to grow; this growth, however, is curtailed by diffusion and large-scale mixing which transport the excess of α out of δV. As the rate of growth of α due to the chemical reactions is proportional to δV, whereas depletion is proportional to the surface area of δV, there is a 'nucleation volume' V_c below which α cannot grow. Within this volume V_c, homogeneity is maintained. Diffusion alone can maintain homogeneity over a length scale $l_D \simeq \sqrt{D/B(\lambda - \lambda_c)}$, D being the diffusion coefficient[26,27]. In our numerical simulation, in stage III, $B(\lambda - \lambda_c) \leq 10^{-11}\ s^{-1}$, and with $D \sim 10^{-5}\ cm^2\ s^{-1}$ we see that $\lambda_D \sim 10^3$ cm. Also, stages II and III are traversed in ~6,000 yr, during which we may expect homogenization due to large-scale mixing to be on an oceanic scale. We assume this volume V_c to be at least 4×10^9 l (1 km × 1 km × 4 m) for our estimate of ε_1. As indicated by the fluctuating trajectory in Fig. 1, by the time stage IV is reached, if the system is already well within the region of attraction of the favoured (upper) branch, it becomes increasingly improbable for a fluctuation in α, occurring at least over a volume V_c, to be large enough to reach the unfavoured (lower) branch.

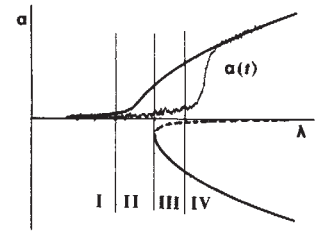

Fig. 1 A sample trajectory of α in equation (1) as λ increases through the critical point (fluctuations exaggerated). Solid line, stable steady states; dashed line, unstable steady state. Stages I-IV are explained in the text.

To obtain the probability for the selection of branches, we study the Fokker-Planck[28,29] equation associated with equation (1), which describes the evolution of the probability density $P(\alpha, t)$ of α:

$$\frac{\partial P}{\partial t} = -\frac{\partial}{\partial \alpha}(-A\alpha^3 + B(\lambda(t) - \lambda_c)\alpha + Cg)P(\alpha, t) + \left(\frac{\varepsilon}{2}\right)\frac{\partial^2}{\partial \alpha^2}P(\alpha, t) \qquad (2)$$

where $\varepsilon = \varepsilon_1 + (C'\eta)^2$. We suppose, at $t = 0$, λ is well below the critical point and is gradually increasing. Fluctuations in λ have an insignificant role in the process of selection[21], so we ignore them in our theoretical discussion, though not in our numerical simulation of the above model shown in Fig. 2. From equation (2) it follows that, for λ well below λ_c, $P(\alpha, t)$ is essentially a gaussian whose centre is at $\bar{\alpha} \simeq Cg/B(\lambda_c - \lambda)$, very close to zero (stage I in Fig. 1). As λ increases at a reasonable rate ($\sim 10^{-5}\ M^2\ (10^4\ yr)^{-1}$ for the model) in the vicinity of the critical point, $P(\alpha, t)$ is still a gaussian, but it begins to relax very slowly to the stationary distribution. Thus, in this stage (stages II and III in Fig. 1), $P(\alpha, t)$ is vanishingly small for large α and hence the $-A\alpha^3$ term may be neglected in comparison with the other terms.

For selection, then, we need only consider

$$\frac{\partial P}{\partial t} = -\frac{\partial}{\partial \alpha}(B(\lambda(t) - \lambda_c)\alpha + Cg)P(\alpha, t) + \left(\frac{\varepsilon}{2}\right)\frac{\partial^2}{\partial \alpha^2}P(\alpha, t) \qquad (3)$$

When $\lambda \simeq \lambda_c$, the term $B(\lambda - \lambda_c)\alpha$, for $\alpha \ll 1$, also becomes small compared with Cg. Here we have a gaussian whose peak is shifting at a constant rate Cg, but whose width is also increasing

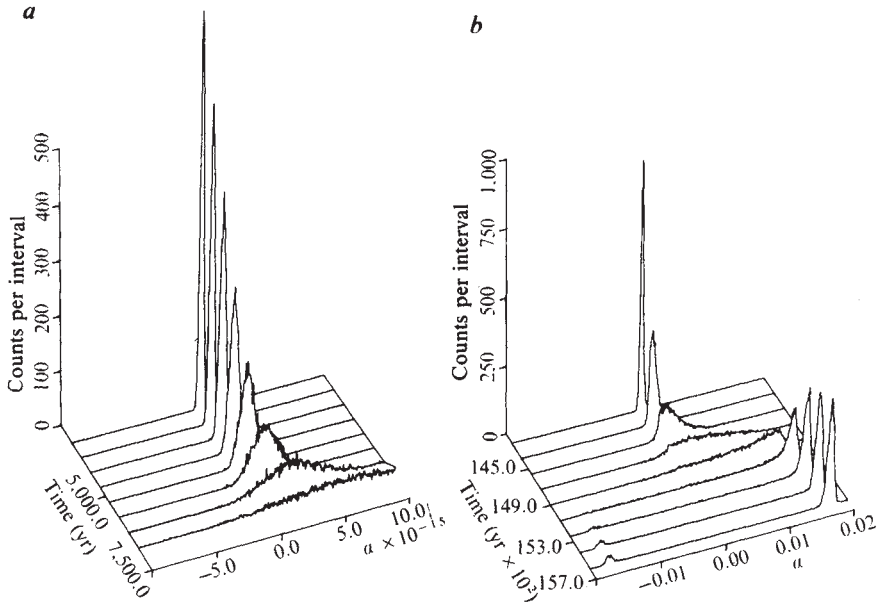

Fig. 2 Results of simulation of equation (2) by 5,000 sample trajectories of equation (1), with $\lambda(t) = \lambda_0 + \gamma t + 0.05 \times \lambda_c \times f(t)$, where $\lambda_0 = 0.8 \times 10^{-5}\ M^2$, $\gamma = 3.171 \times 10^{-17}\ M^2\ s^{-1}$, and $f(t)$ is normalized gaussian noise; t goes from 0 to 15,600 yr. Other parameters are as given in the text. Each curve is a histogram of the number of times $\alpha(t)$ fell within an interval 1/400 of full α scale for the given t. *a*, $P(\alpha)$ drifting and spreading while λ is near λ_c, which here occurs at $t = 3{,}000$ yr. *b*, $P(\alpha)$ spreading and splitting for $\lambda \gg \lambda_c$. Note the change of scale in α by 10^{12} between *a* and *b*, because of which the number of trajectories per interval has sharply increased in *b*.

because of the 'diffusion term' containing ε. In a time interval T, the drift of the peak will be CgT, while the increase in the width will be $\sqrt{\varepsilon T}$. Thus, for sufficiently large T, even when $Cg \ll \sqrt{\varepsilon}$, CgT can exceed $\sqrt{\varepsilon T}$, which implies that much of $P(\alpha, t)$ will drift into the region $\alpha > 0$ (for $Cg > 0$). This is the heart of the selection mechanism. Now, as λ goes beyond λ_c (stage IV in Fig. 1), the term $B(\lambda - \lambda_c)$ is positive and will cause $P(\alpha, t)$ to spread out rapidly on either side. $P(\alpha, t)$, thus split into two parts, will accumulate around the macroscopic steady states because of the term $-A\alpha^3$; note, however, that by the time this term becomes important, how much of $P(\alpha, t)$ will have evolved into $\alpha > 0$ and $\alpha < 0$ regions will already have been determined. Thus, equation (3) is all we need to calculate the probability of branch selection—an approximation well supported by the numerical solution of the complete equation.

The solution to equation (3), well known[29,30] for constant λ, can be extended to time-dependent λ. With $P(\alpha,0) = \delta(\alpha - \alpha_0)$, the solution $P(\alpha, t|\alpha_0)$ is a gaussian that is drifting and spreading

$$P(\alpha, t|\alpha_0) = \frac{1}{[\pi z(t)]^{1/2}} \exp\left[\frac{(\alpha - \bar{\alpha}(t))^2}{z(t)}\right] \tag{4}$$

where

$$\bar{\alpha} = \alpha_0 \exp(w(t)) + Cg \exp w(t) \int_0^t \exp(-w(t'))\mathrm{d}t'$$

in which

$$w(t) = \int_0^t B(\lambda(t') - \lambda_c)\, \mathrm{d}t'$$

and

$$z(t) = 2\varepsilon \int_0^t \exp(2\int_{t'}^t B(\lambda(t'') - \lambda_c)\, \mathrm{d}t'')\, \mathrm{d}t'$$

For the probability of selection of the $\alpha > 0$ chiral steady state, P_+, we have: $P_+ = \mathrm{Lt}_{t\to\infty} \int_0^\infty P(\alpha, t/\alpha_0)\, \mathrm{d}\alpha$. Because $P(\alpha, t|\alpha_0)$ is a gaussian and $\alpha_0 \approx 0$, we may write

$$P_+(t) = \frac{1}{\sqrt{2\pi}} \int_{-\infty}^{N} \mathrm{e}^{-x^2/2}\, \mathrm{d}x \tag{5}$$

where

$$N = Cg\left[\exp w(t) \int_0^t \exp(-w(t'))\, \mathrm{d}t'\right] \Big/ \sqrt{z(t)/2} \tag{6}$$

gives the number of standard deviations by which the peak of $P(\alpha, t)$ has drifted from the origin. Now, if we let $\lambda = \lambda_0 + \gamma t$ (λ_0 well below λ_c), for $t \to \infty$, we get

$$N = Cg(\varepsilon/2)^{-1/2}(B\gamma/\pi)^{-1/4} \tag{7}$$

Thus, equations (7) and (5) give the required probability for the selection of a branch resulting from a chiral interaction.

For the biomolecular context we consider the above model with kinetic constants $k_1 = 5 \times 10^{-5}\ M^{-1}\ s^{-1}$, $k_2 = 2.5 \times 10^{-5}\ M^{-2}\ s^{-1}$, $k_3 = 10^{-3}\ M^{-1}\ s^{-1}$, $k_{-1} = 2.5 \times 10^{-10}\ s^{-1}$ and $k_{-2} = 1.25 \times 10^{-10}\ M^{-1}\ s^{-1}$. With these values the coefficients of equation (1) are: $A = 1.7 \times 10^{-7}\ M^{-2}\ s^{-1}$, $B = 2.5 \times 10^{-5} M^{-2}\ s^{-1}$, $C = 2.5 \times 10^{-10}\ M\ s^{-1}$ and $\lambda_c = 1.0 \times 10^{-5}\ M^2$; all concentrations are $\sim 10^{-3}$ M or less during the process of selection and $[X] \sim 10^{-2}$ M well above λ_c. If we suppose [S] and [T] are increasing slowly so that $\lambda \equiv [S][T]$ increases from $0.5\,\lambda_c$ to $1.5\,\lambda_c$ in 10,000 yr, then $\gamma = 3.2 \times 10^{-17}\ M^2\ s^{-1}$. For $\varepsilon_1 = Q/VN_A$, $Q = (k_1\lambda_c)/2$ for the model [14], and we take $V = 4 \times 10^9$ l as explained above, so that $\varepsilon_1 \simeq 10^{-43}\ M^2\ s^{-1}$. Using the results of Mason and Tranter for WNC[15], we take $g \simeq 10^{-17}$, which makes $Cg = 2.5 \times 10^{-27}$. For the magnitude of the random chiral influences, we take $C'\eta = 3 \times 10^{-22}$, an estimate explained below. Using these values in equation (7) we get $N \simeq 2.0$, which implies $P_+ \simeq 0.98$, a 98% chance that the enantiomer favoured by WNC will emerge dominant even though the r.m.s. values of the random chiral influences are five orders of magnitude larger. Such sensitivity cannot be realized if the system does not evolve through the critical point.

To check the validity of our approximation of using equation (3) instead of equation (2), we numerically modelled the stochastic equation (1), with $\lambda = \lambda_0 + \gamma t + 0.05\,\lambda_c f(t)$, $f(t)$ being a gaussian noise. The results are shown in Fig. 2. For easier graphical visualization, we set $\varepsilon = 3.9 \times 10^{-43}$. Then, according to equation (5), $N = \sqrt{2}$, implying $P_+ = 0.921$ selectivity. Figure 2 is the result of averaging 5,000 trajectories and gives a $P_+ = 0.916$ in good agreement with the analytical result. If λ evolves extremely slowly, the approximation of using equation (3) is not valid. In the limit of infinitely slow λ_D, the results in refs 14, 16 can be used; for the intermediate region no analytical results exist.

For the estimate of the r.m.s. value of the random environmental factors, we take circularly polarized light in the ultraviolet range to be typical. (Hardly any reliable data exist for other effects.) Chirally selective photochemical effects of circularly polarized light are well known[31–33]. In our model, let us assume that chirally selective degradation of X (back reaction of reaction

(i)), at a rate $k'[X]$, occurs with a mean life of about 3,000 yr, that is $k' \simeq 10^{-11}\ s^{-1}$ for the average solar intensity. (Note, this is also the racemization rate.) For 100% circularly polarized light, the rate of decay of one of the enantiomers is faster by a factor $s \simeq 10^{-3}$ or less for most molecules[32,33], although there are exceptions[34]. Only a fraction $q \simeq 10^{-3}$ of the solar intensity at dawn and dusk is found to be circularly polarized in the infrared frequencies and is at least an order of magnitude smaller for the ultraviolet[35]. The sense of polarization depends on the direction and on the average it is zero. Considering the reduction of q for daylight intensities and attenuating factors in a large body of water, we may take $q_{rms} \simeq 10^{-6}$ with a correlation time $\tau \simeq 10^3$ s. On the evolutionary timescale of 10^{10}–10^{12} s considered here, this may be considered white noise of strength $\sqrt{2\tau}\, q_{rms}$ (equivalent to diffusion constant of $(1/2\tau)$ steps per unit time, each of length $2\tau q_{rms}$). Thus, the rate of asymmetric synthesis is $k'[X_{L(D)}]qs$; when q is a fluctuating quantity it may be represented by a gaussian white-noise term $C'\eta f_2(t)$, with $C'\eta = k'[([X_L]+[X_D])/2]s\sqrt{2\tau}\, q_{rms}$. By analogy with Cg, we may define $C' \equiv k'([X_L]+[X_D])/2$ and $\eta = s\sqrt{2\tau}\, q_{rms}$. With the above numerical values and $[X] \simeq 10^{-3}$ M, $C'\eta \simeq 3 \times 10^{-22}$, the value used in our numerical estimates.

We thank Professors I. Prigogine, J. Whitesell, C. Van den Broeck and M. Malek-Mansour for stimulating and useful discussions. D.K.K. thanks the US Department of Energy, Basic Energy Sciences (grant DE-AS05-81ER10947) and G.W.N. thanks the Welch Foundation and the International Paper Company for financial support.

Received 5 November 1984; accepted 23 January 1985.

1. Mason, S. F. *Int. Rev. phys. Chem.* **3**, 217-241 (1983); *Nature* **311**, 19-23 (1984).
2. Elias, W. E. *J. chem. Educ.* **49**, 448-454 (1972).
3. Miller, S. W. & Orgel, L. E. *The Origin of Life on Earth* (Prentice-Hall, New Jersey, 1974).
4. Fox, S. W. & Dose, K. *Molecular Evolution and the Origin of Life* (Dekker, New York, 1977).
5. Frank, F. C. *Biochim. biophys. Acta* **11**, 459-463 (1953).
6. Seelig, F. F. *J. theor. Biol.* **31**, 335-361 (1971).
7. Decker, P. *J. molec. Evol.* **4**, 49-65 (1974).
8. Zel'dovich, Ya. B., Saakyan, D. B. & Sobel'man, I. I. *Pis'ma Zh. eksp. teor. Fiz.* **25**, 106-109 (1977) (*J. exp. theor. phys. Lett.* **25**, 94-98).
9. Hegstrom, R. A., Rein, D. W. & Sandars, P. G. H. *J. chem. Phys.* **73**, 2329-41 (1980).
10. Thiemann, W. (ed.) *Origins Life* **11**, 1-194 (1981).
11. Keszthelyi, L. *Origins Life* **14**, 375-382 (1984).
12. Mead, C. A. & Moscowitz, A. *J. Am. chem. Soc.* **102**, 7301-7302 (1980).
13. Peres, A. *J. Am. chem. Soc.* **102**, 7389-7390 (1980).
14. Kondepudi, D. K. & Nelson, G. W. *Physica* **125A**, 465-496 (1984).
15. Mason, S. F. & Tranter, G. E. *JCS chem. Commun.*, 117-119 (1983); *Molec. Phys.* **53**, 1091-1111 (1984).
16. Kondepudi, D. K. & Nelson, G. W. *Phys. Rev. Lett.* **50**, 1023-1026 (1983).
17. Kondepudi, D. K. & Prigogine, I. *Physica* **107A**, 1 (1981).
18. Sattinger, D. H. *Lecture Notes in Mathematics* No. 762 (Springer, Berlin, 1979).
19. Mangel, M. *J. chem. Phys.* **69**, 3697-3708 (1978).
20. Keizer, J. *J. chem. Phys.* **69**, 2609-2620 (1978).
21. Kondepudi, D. K. in *Fluctuations and Sensitivity in Nonequilibrium Systems* (eds Horsthemke, W. & Kondepudi, D. K.) 204-213 (Springer, Berlin 1984).
22. Kondepudi, D. K. & Nelson, G. W. *Phys. Lett.* **106A**, 203-206 (1984).
23. Mangel, M. *Phys. Rev.* **A24**, 3226-3238 (1981).
24. Morozov, L. L., Kuz'min, V. V. & Gol'danskii, V. I. *Origins of Life* **13**, 69-101 (1983).
25. Morozov, L. L., Kuz'min, V. V. & Gol'danskii, V. I. *Pis'ma Zh. exsp. teor. Fiz.* **39**, 344-345 (1984); *JETP Lett.* **39**, 414-416 (1984).
26. Nicolis, G. & Prigogine, I. *Self Organization in Nonequilibirum Systems* (Wiley, New York, 1977).
27. Nicolis, G. & Malek-Mansour, M. *Phys. Rev.* **A29**, 2845-2853 (1984).
28. Nitzan, A., Ortoleva, P., Deutch, J. & Ross, J. *J. chem. Phys.* **61**, 1056-1074 (1974).
29. Van Kampen, N. G. *Stochastic Processes in Physics and Chemistry* (North-Holland, Amsterdam, 1981).
30. Uhlenbeck, G. E. & Ornstein, L. S. *Phys. Rev.* **36**, 824-841 (1930).
31. Kuhn, W. & Braun, F. *Naturwissenchaften* **17**, 227-228 (1929).
32. Kagan, H. B. *et al Tetrahedron Lett.* **27**, 2479-2482 (1971).
33. Kagan, H. B., Balavoine, G. & Moradpour, A. *J. molec. Evol.* **4**, 41-48 (1974).
34. Flores, J. J., Bonner, W. A. & Massey, G. A. *J. Am. chem. Soc.* **99**, 3622-3624 (1977).
35. Angel, J. R. P., Illing, R. & Martin, P. G. *Nature* **238**, 389-390 (1972).

Presynaptic neurones may contribute a unique glycoprotein to the extracellular matrix at the synapse

Pico Caroni, Steven S. Carlson, Erik Schweitzer & Regis B. Kelly

Department of Biochemistry and Biophysics, University of California, San Francisco, California 94143, USA

As the extracellular matrix at the original site of a neuromuscular junction seems to play a major part in the specificity of synaptic regeneration[1–5], considerable attention has been paid to unique molecules localized to this region[6–11]. Here we describe an extracellular matrix glycoprotein of the elasmobranch electric organ that is localized near the nerve endings. By immunological criteria, it is synthesized in the cell bodies, transported down the axons and is related to a glycoprotein in the synaptic vesicles of the neurones that innervate the electric organ. It is apparently specific for these neurones, as it cannot be detected elsewhere in the nervous system of the fish. Therefore, neurones seem to contribute unique extracellular matrix glycoproteins to the synaptic region. Synaptic vesicles could be involved in transporting these glycoproteins to or from the nerve terminal surface.

Cholinergic synaptic vesicles have been purified to near homogeneity from the electric organs of elasmobranchs[12,13] and have been used to generate nerve-terminal-specific antiserum[14,15]. Using synaptic vesicles purified from the electric organ of *Discopyge ommata* as antigen, we have generated monoclonal antibodies to unique vesicle components copurifying with synaptic vesicle contents during size fractionation. The vesicle-specific monoclonal antibodies define at least four different antigenic determinants (SV1–SV4). The SV1 region is part of the same proteoglycan-like molecule that binds monoclonal antibody tor70 (ref. 16). The other three sites have not yet been described. SV2 is fully accessible to antibody in intact vesicles, whereas the rest become accessible only after sonication or detergent treatment, and so are presumably exposed on the inside of the vesicle[17].

The relative concentration of each antigenic determinant was measured by quantitative immunoblotting of synaptic vesicles (Table 1). All four antigens are present in electric organ synaptosomes at about one-tenth of the concentration in vesicles, which is as expected because acetylcholine and ATP in the vesicles have ~10 times higher concentrations per mg protein[12] than in synaptosomes[18]. When the relative concentrations of all four determinants were measured on homogenates of electric organ (Table 1), SV2 and SV3 had low specific activities, as expected from earlier calculations[12]. The specific activity in the electric organ of the SV4 antigenic sites, however, was ~10 times higher than expected, suggesting that ~90% of it is not in synaptic vesicles. The SV4 site, unlike the other three, is found in high concentrations in an extracellular matrix fraction of the electric organ, where the specific activity is higher than in synaptic vesicles (Table 1). As 77% of the total SV4 (but only 2.1% of the total protein) is recovered in the extracellular matrix, most of the SV4 antigen in electric organ may not be in synaptic vesicles, but in the matrix.

The molecules carrying SV4 and SV1 are highly restricted in their location, whereas the SV2 and SV3 antigens occur in all nerve terminals of the electric fish. In homogenates of brain and spinal chord SV4 and SV1 were less than 2% of the value predicted from the amount of SV2 and equal to background levels measured using liver homogenates. By immunofluorescence the cell bodies of the electromotor nucleus contain large amounts of the SV2, SV1 and SV4 sites, whereas synapses in other brain regions have SV2 but no detectable SV4 or SV1 (K. Buckley, unpublished observations), hence the SV4 and SV1 antigens are restricted to electromotor nucleus neurones.

The molecule in synaptic vesicles carrying the SV4 site has a heterogeneous mobility and its antigenicity is destroyed by exposure to conditions[19] that remove carbohydrate side chains from proteins (Fig. 1). The molecule thus has the properties of a glycosylated protein whose antigenicity is associated with oligosaccharides. The SV4 antigen from the extracellular matrix fraction shows the same heterogeneous electrophoretic mobility, and the same susceptibility to mild proteolysis and sensitivity